Electronic Supplementary Information

Sustainable Iron Production via Highly Efficient Low-Temperature Electrolysis of 3D Conductive Colloidal Electrodes

Panya Thanwisai[a, †], Zeyi Yao[a, †], Muntasir Shahabuddin[b], Jiahui Hou[a], Jinzhao Fu[a], Adam C. Powell IV[a] and Yan Wang[*a]

[a]*Department of Mechanical and Materials Engineering, Worcester Polytechnic Institute, Worcester, MA, 01609, USA*

[b]*Department of Chemical Engineering, Worcester Polytechnic Institute, Worcester, MA, 01609, USA*

[*]*E-mail: yanwang@wpi.edu*

[†]*These authors contributed to this work equally.*

Experimental sections

Preparation of colloidal electrode: nanosized Fe_2O_3 powder (Sigma Aldrich) and nanosized carbon powder (Ketjen black 600D), in a weight ratio of 9:1, were mixed by a planetary ball milling (ball-to-powder ratio = 10:1) for 2h at 400 rpm to form Fe_2O_3/C aggregates. The obtained Fe_2O_3/C powder was then ground with NaOH pellets (VWR) and H_2O using mortar and pestle until the slurry became homogeneous, followed by adding ∼20 μl of 3,6-dioxa-1.8 octanedithiol organic additive (TCI, >97%) and ∼10 mg of $Na_2S \cdot xH_2O$ inorganic additives (Sigma Aldrich) to help suppress H_2 evolution and promote the reduction reaction.[1, 2] The ratio of Fe_2O_3/C powder: NaOH: H_2O is 15 wt%: 42.5 wt%: 42.5 wt%. The homogenous mixture was then further mixed by a speed mixer at 400 rpm and the colloidal electrode was finally obtained.

Electrolysis experiment set up: The colloid was applied onto a cathode current collector (Ni foam/Ti foil) with a diameter of 24 mm and then put in a polypropylene sample holder. A filter paper separator (VWR, 25 μm pore size) was pressed tightly against the electrode. Ni foam was arranged on the top of the separator serving as an anode. The electrochemical cell is a two-electrode configuration. The entire electrolysis cell was immersed in an electrolysis reactor containing 150 mL of 50 wt% NaOH solution electrolyte. Then, the reactor was heated to 100 °C and stirred continuously to keep the temperature uniform and facilitate OH^- ion transfer between the two electrodes. A voltage of -1.7V was applied to the electrolysis cell by a potentiostat (EC-lab, biologic). The theoretical capacity calculated based on the Faraday's law shown in equation (S1):

$$Q = \frac{mFz}{3600 \times Mw}$$

(S1)

where Q is the theoretical capacity (mAh), m is the mass of Fe_2O_3 in the slurry (g), F is Faraday's constant (96485 s A/mol), z is the numbers of electrons transferring in the redox reaction (z=6 from equation 4), M_w is the molecular weight of Fe_2O_3 (159.69 g/mol).
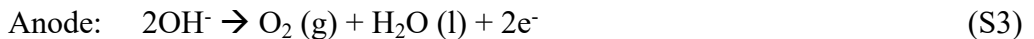
Electrolyzed Fe powder collection and separation: After the electrolysis reaction finished, the electrolyzed product was collected from the sample holder and thereafter washed with distilled water. Sonication was applied to further wash the product. After sonication, the powder was filtered using a vacuum pump followed by thoroughly washing with distilled water and ethanol. The final powder was then dried at 60°C in a vacuum oven overnight. In the separation process, Fe powders were dispersed in ethanol and sonicated for 40 min. During sonication, a magnet was dipped into the solution so that Fe powder would be attached to the magnet by a magnetic force. The step was repeated several times to obtain Fe powder as much as possible. The obtained Fe powders were further dried at 60°C in a vacuum oven for 12h.

Characterizations: X-ray powder diffraction (XRD) was performed on PANalytical Empyrean to study material structure, identify impurity phases, and preliminarily determine the purity of the obtained Fe powder by peak analysis. Scanning electron microscopy (SEM) and energy dispersive X-ray spectroscopy (EDS) were carried out on JEOL JSM 7000F to examine material morphology and chemical compositions. Focused ion beam scanning electron microscopy (FIB-SEM) with EDS with line scanning mapping performed on Thermo Scientifc™ Scios™ 2 DualBeam™ was utilized to investigate chemical compositions inside the produced Fe particles. The BET surface area measurement was done using N_2 gas adsorption in micromeritics®. The de-gassing

temperature was 120 °C. The viscosity test was performed on a MCR 302 WESP (Anton Paar) with cone-plate (CP25-1/TG) configuration of 1° cone angle and 25 mm diameter. Inductively coupled plasma optical emission spectroscopy (ICP-OES) using Horiba Ultima 2 was conducted to analyze elemental compositions of Fe powders.
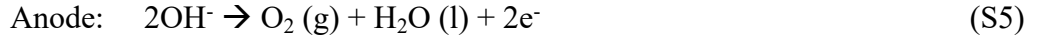
Electrolysis of AgO, CuO and NiFe$_2$O$_4$

Electrolysis of AgO: Firstly, AgO powders (Sigma Aldrich) were mixed with NaOH solution without C powder due to their excellent electrical conductivity. Then the AgO suspension was transferred to the Ni foam substrate for use as a cathode. The electrolysis condition is using 50 wt% NaOH solution and -1.2V of applied voltage. The electrolysis was operated at 95 °C and prolonged until reaching 1x theoretical capacity applied. After the electrolysis, the produced Ag powders were washed thoroughly with DI water and ethanol and then dried at 60 °C overnight in a vacuum oven before use. The electrochemical reduction of AgO to Ag was proposed according to the following equations.
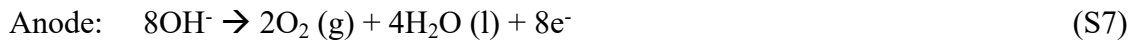
$$\text{Cathode:} \quad AgO \text{ (s)} + H_2O \text{ (l)} + 2e^- \rightarrow Ag \text{ (s)} + 2OH^- \tag{S2}$$

$$\text{Anode:} \quad 2OH^- \rightarrow O_2 \text{ (g)} + H_2O \text{ (l)} + 2e^- \tag{S3}$$

Electrolysis of CuO: Similar to Fe$_2$O$_3$, CuO powders (Sigma Aldrich) were first mixed with C (9:1 mass ratio) by ball milling to form CuO/C aggregates by ball milling at 400 rpm for 2 h. The aggregates were mixed with NaOH solution in the same mass ratio as the Fe$_2$O$_3$ slurry. Then the CuO/C suspension was transferred to the Ni foam substrate for use as a cathode. The electrolysis condition is using 50 wt% NaOH solution and -1.2V of applied voltage. The electrolysis was operated at 95 °C and prolonged until reaching 1x theoretical capacity applied. After the electrolysis, the produced Ag powders were washed thoroughly with DI water and ethanol and

then dried at 60 °C overnight in a vacuum oven before use. The electrochemical reduction of CuO to Cu was proposed according to the following equations.

$$\text{Cathode:} \quad CuO\ (s) + H_2O\ (l) + 2e^- \rightarrow Cu\ (s) + 2OH^- \tag{S4}$$

$$\text{Anode:} \quad 2OH^- \rightarrow O_2\ (g) + H_2O\ (l) + 2e^- \tag{S5}$$

Electrolysis of NiFe$_2$O$_4$: Before slurry making, NiFe$_2$O$_4$ powders were first synthesized by a facile hydrothermal method. Stoichiometric NiCl$_2$ · 6H$_2$O (Sigma Aldrich) and FeCl$_3$ (Sigma Aldrich, 97%) were dissolved in 40 mL of DI water and then stirred continuously for 2h at room temperature until the solution was homogenous. After that, stoichiometric NaOH solution was added to the first solution dropwise with continuous stirring for 1h. The mixture was then transferred to the 50 mL Teflon tube before heating at 220 °C for 15 h. The produced NiFe$_2$O$_4$ powders were filtered and dried at 80 °C for 12 hours before use.

In order to prepare NiFe$_2$O$_4$/C aggregates, the synthesized NiFe$_2$O$_4$ powders were ball-milled with C in a 9:1 mass ratio at 400 rpm for 2h. Then the NiFe$_2$O$_4$/C aggregates were mixed with NaOH solution in the same mass ratio as the Fe$_2$O$_3$ slurry. The homogenous NiFe$_2$O$_4$/C slurry was then transferred to the Ni foam cathode substrate for an electrolysis experiment. In this experiment, the electrolysis was operated at 100 °C in 50 wt% NaOH solution. The voltage of -1.85V was applied to run the reaction until it reached 4x the theoretical capacity. The electrochemical reduction of NiFe$_2$O$_4$ to FeNi alloy was proposed according to the following equations.

$$\text{Cathode:} \quad NiFe_2O_4\ (s) + 4H_2O\ (l) + 8e^- \rightarrow NiFe_2\ (s)^* + 8OH^- \tag{S6}$$

$$\text{Anode:} \quad 8OH^- \rightarrow 2O_2\ (g) + 4H_2O\ (l) + 8e^- \tag{S7}$$

*Note that the alloy products can be in different phases.

After the electrolysis finishes, the washing and separation processes follow the methods used in the Fe_2O_3 electrolysis.

Electrical conductivity measurement

To measure the electrical conductivity of Fe_2O_3 colloidal electrodes, a coin cell configuration with a slurry holder was designed as shown in Fig. S1a. The slurry holder made of polypropylene (PP) has a depth of 0.1737 cm and a diameter of 0.6732 cm. A constant voltage of -0.1V was controlled between the two electrode surfaces using the chronoamperometric technique. The electrical conductivity was calculated by using Ohm's law as in equation (S8).

$$R = \frac{V}{I}$$
(S8)

Here, R is the electrical resistance (Ω), V is a constant voltage applied (0.1 V), and I is the current passed through the colloids (A). Then, electrical conductivity can be obtained by using equation (S9).

$$\sigma = \frac{L}{RA}$$
(S9)

Where σ is electrical conductivity (S/m), L is the thickness of the holder (0.1737 cm), and A is the area of the holder (0.3559 cm^2).

Energy loss through lead calculation based on Wiedemann Franz Law

$$P + Q = 2I \sqrt{L_{el}T\Delta T}$$
(S10)

where P is electrical resistance energy loss, Q is thermal energy loss through lead, I is cell current, L_{el} is Lorenz number ($2.44 \times 10^{-8} W\Omega K^{-2}$), T is cell temperature, and ΔT is the temperature difference between cell and ambience.

(a) PP slurry holder
Fe$_2$O$_3$ colloids

Spacer

Spring

Cap

(b)
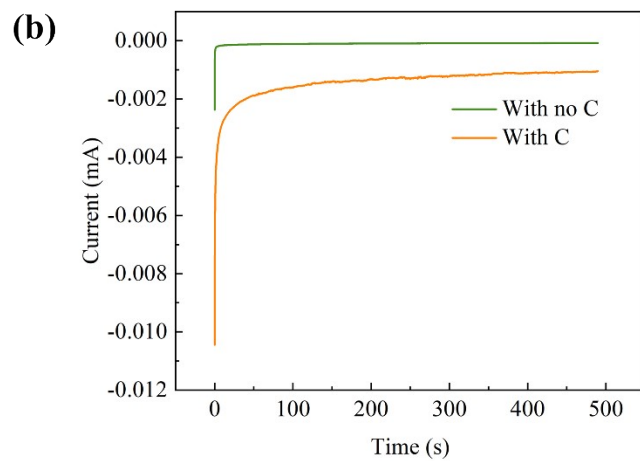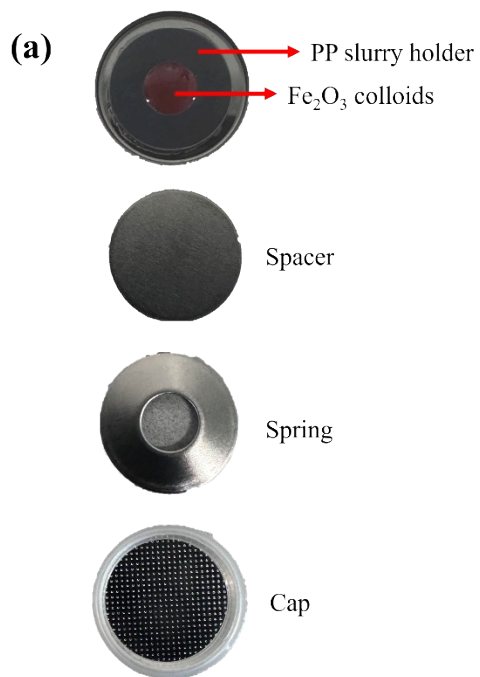
Fig. S1 (a) Coin cell design for electrical conductivity testing of slurry. (b) Current produced at a constant voltage of -0.1V applied.
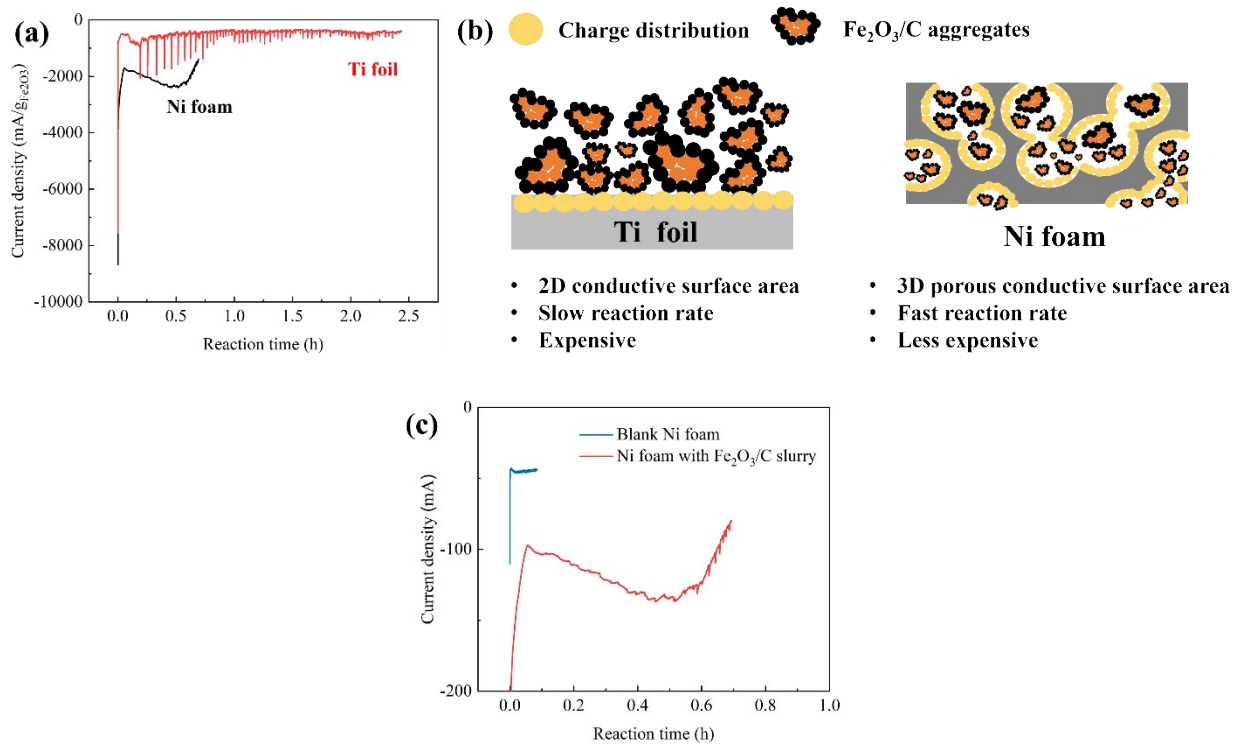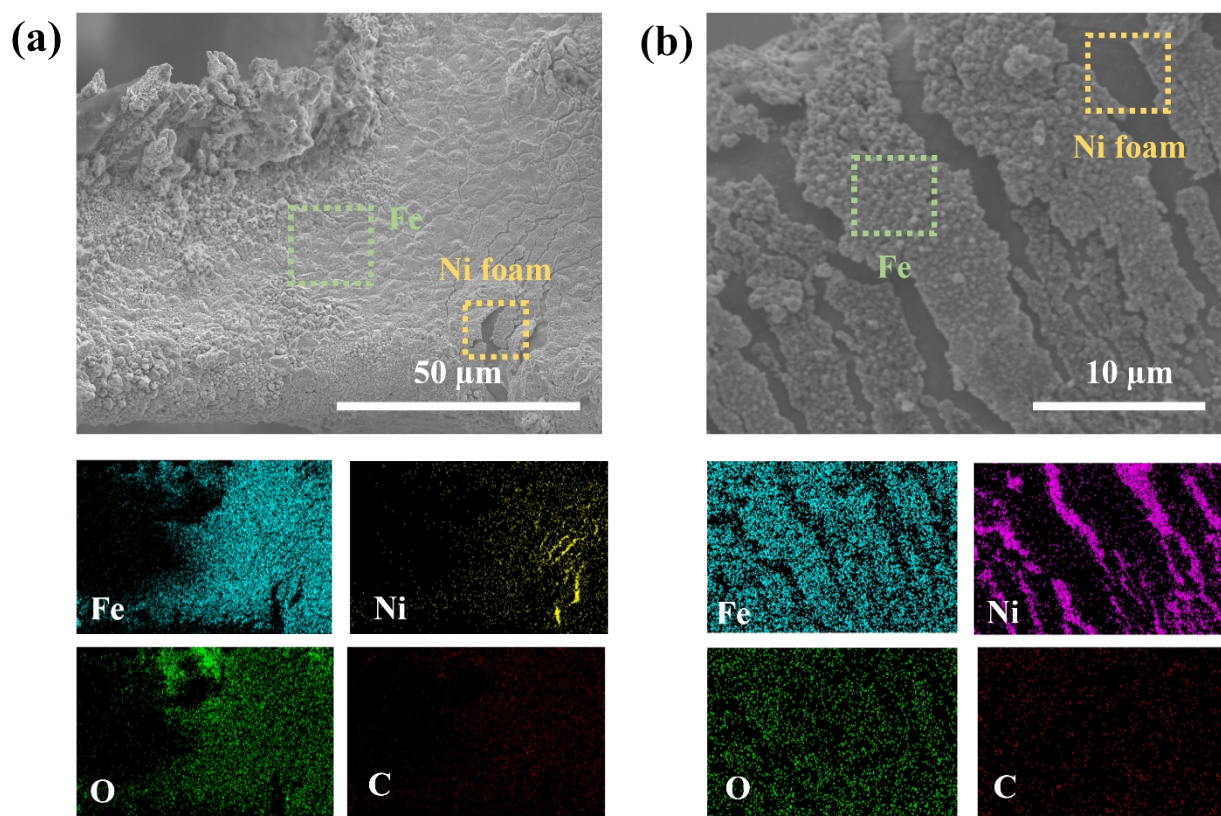
Fig. S2 (a) Electrolysis current vs. reaction time plot obtained from using Ti foil and Ni foam substrate. (b) A schematic illustration showing the charge distribution on Ti foil and Ni foam surfaces during the reduction of Fe_2O_3/C suspension. (c) Current produced from blank Ni foam and Ni foam with Fe_2O_3/C slurry.
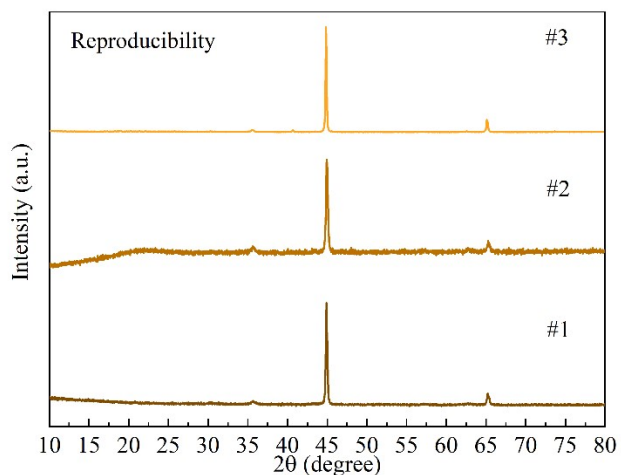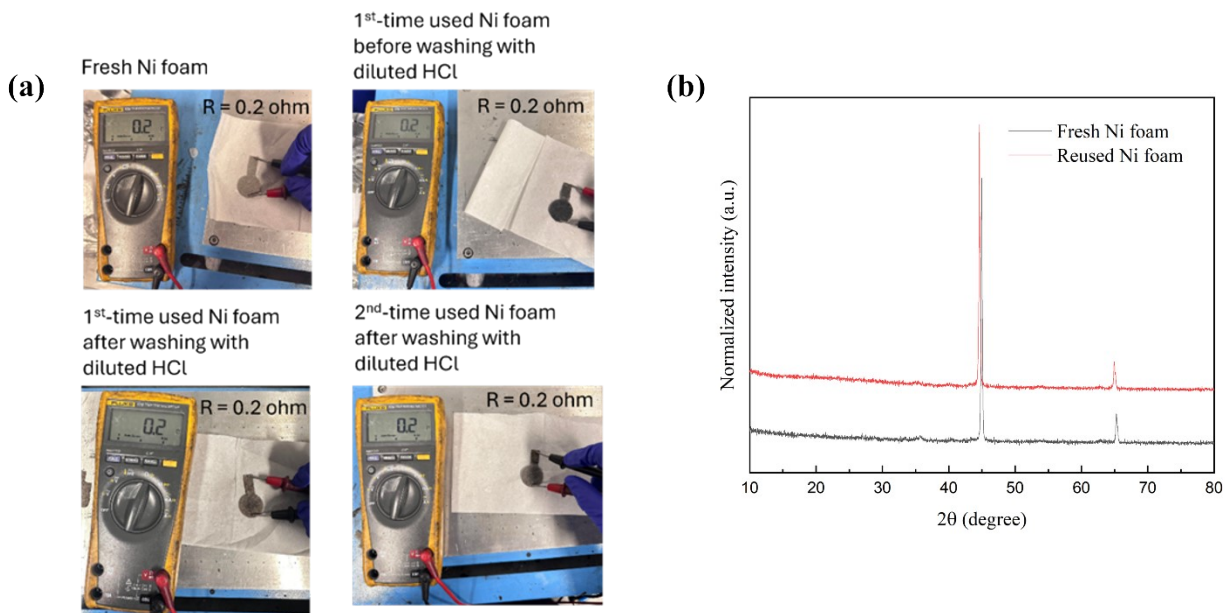
**Fig. S3** XRD pattern of reproduced Fe from the LTE process.

Fig. S4 SEM/EDS images of Ni foam after electrolysis of (a) the colloidal electrode with no C and (b) the colloidal electrode with C.

S9

Fig. S5 (a) Resistance test of Ni foam before and after use. (b) XRD patterns of Fe produced by using fresh and reused Ni foam.

Regarding the concern about reusability of Ni foam, we provide resistance test of Ni foam before and after use as well as purity of Fe produced from using fresh and reused Ni foam. It is seen that Ni foam can be reused to produce high purity Fe. The Fe on the surface of Ni foam can be removed by washing with diluted HCl acid and thoroughly washing with DI water and ethanol. The resistance of the Ni foam remained unchanged after 2-times usage (Fig. S5a). The Fe products obtained from using fresh and reused Ni foam provide similarly high purity (Fig. S5b).
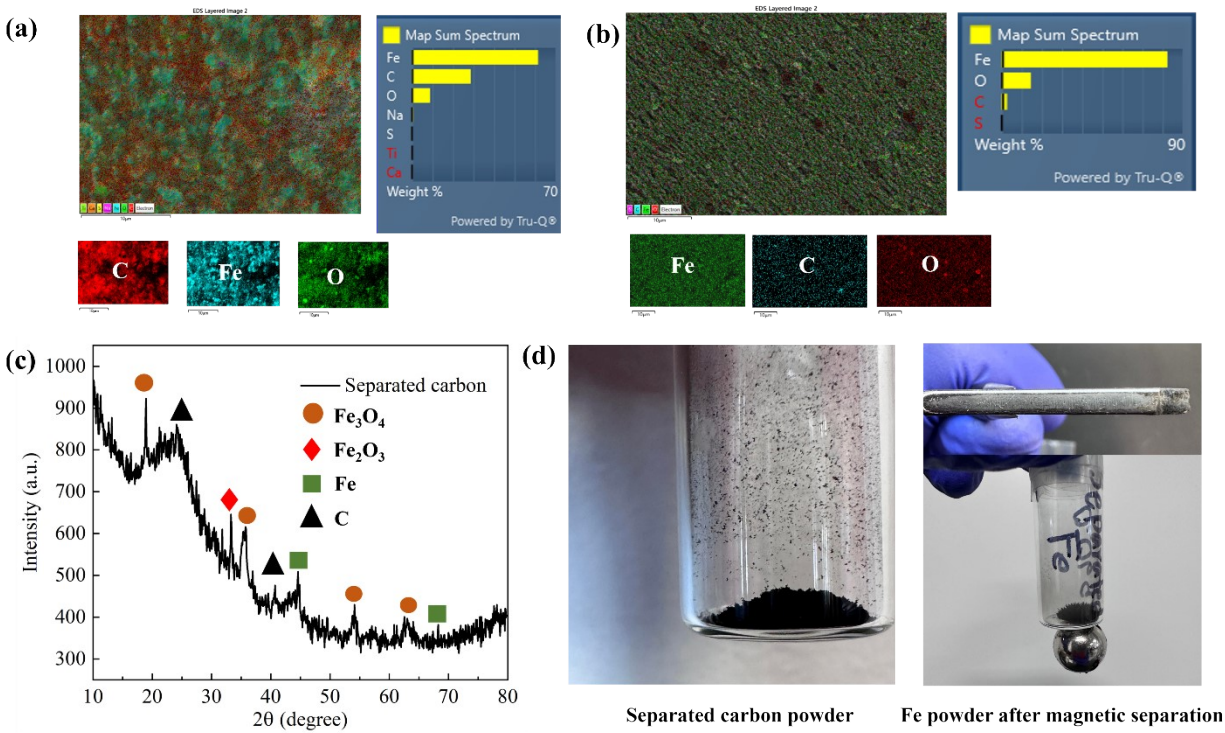
Fig. S6 SEM-EDS of electrolyzed Fe (a) before and (b) after separation. Note that there is a signal of O because of the air exposure during sample preparation and sample transfer. (c) XRD pattern of separated C powders. (d) Photographs of the separated electrolyzed products: separated C powders and Fe powders.
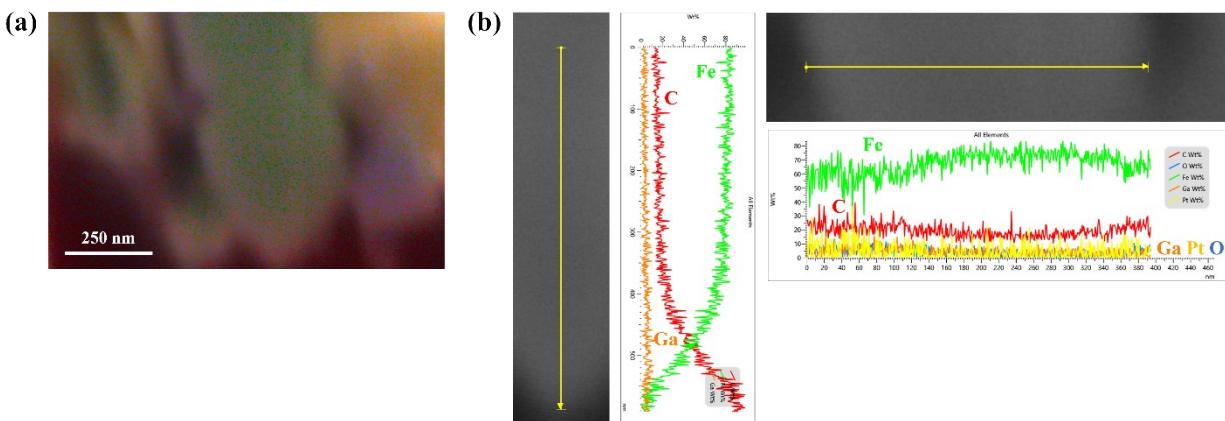
Fig. S7 (a) EDS mappings and (b) line-scanning EDS mappings of cross-sectional Fe particles.
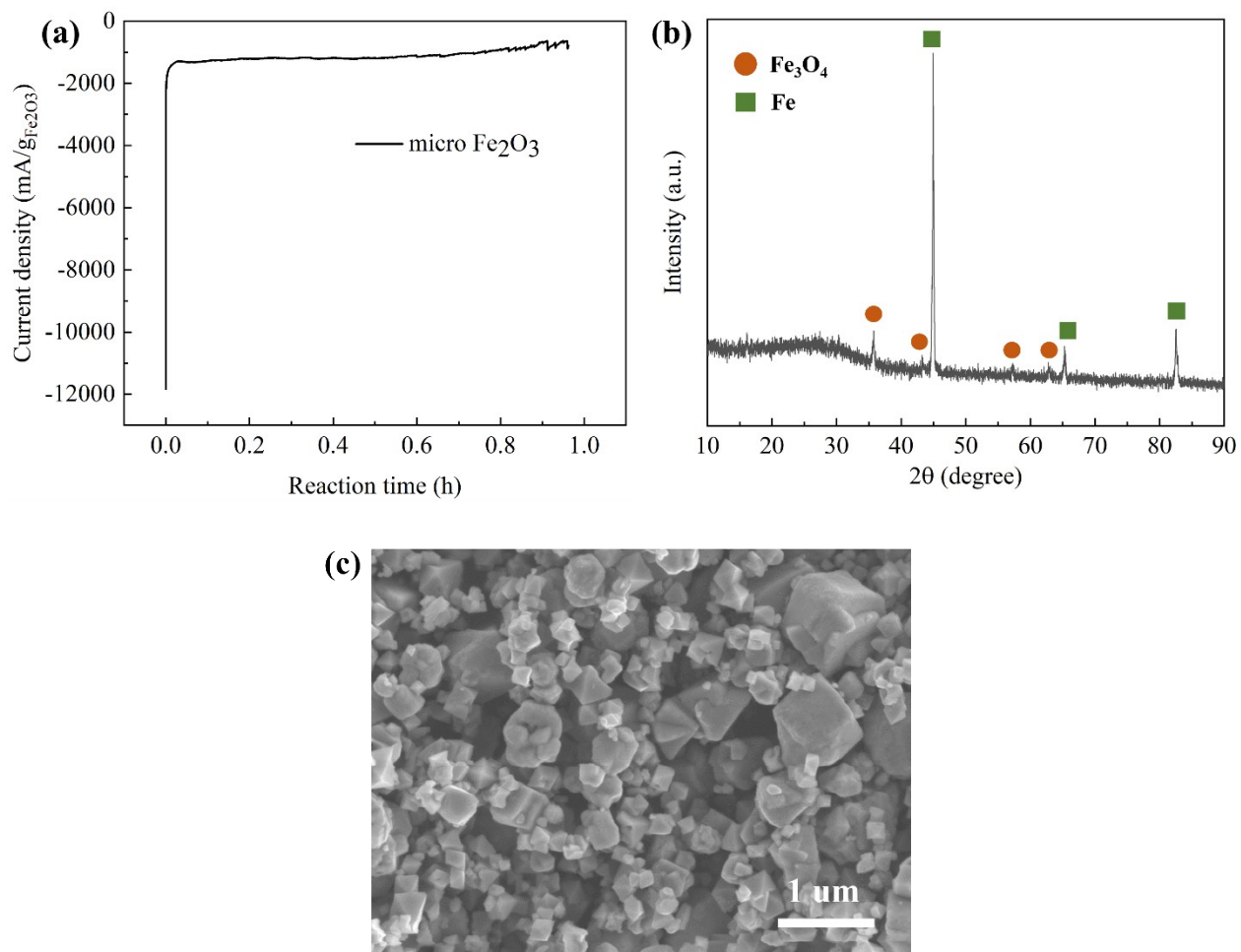
Fig. S8 (a) Electrolysis current vs. reaction time plot with 1-time capacity applied. (b) XRD pattern of electrolyzed product. (c) SEM image of micro Fe_2O_3/C colloidal electrodes.
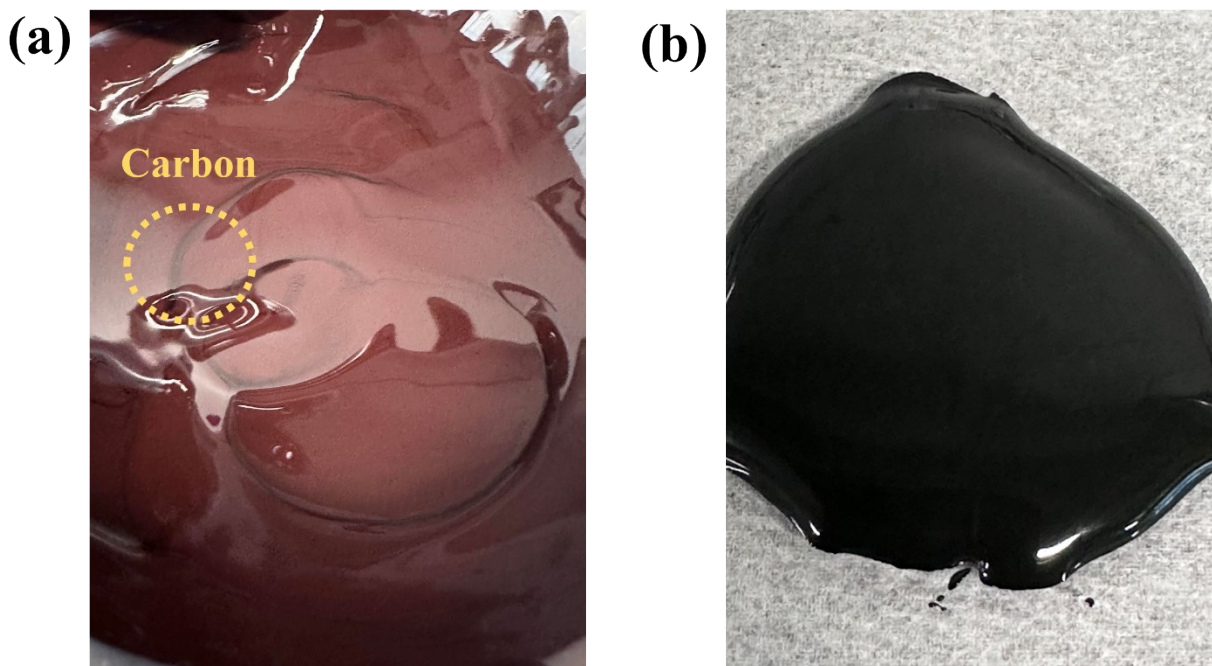
Fig. S9 (a) Fe$_2$O$_3$/C suspension using micro-sized Fe$_2$O$_3$. (b) Fe$_2$O$_3$/C suspension using nano-sized Fe$_2$O$_3$. The phase separation between carbon and Fe$_2$O$_3$ is obviously seen in the micro-sized one where the yellow circle shows the separated carbon phase. In contrast, this phase separation cannot be seen in the nano Fe$_2$O$_3$ slurry.
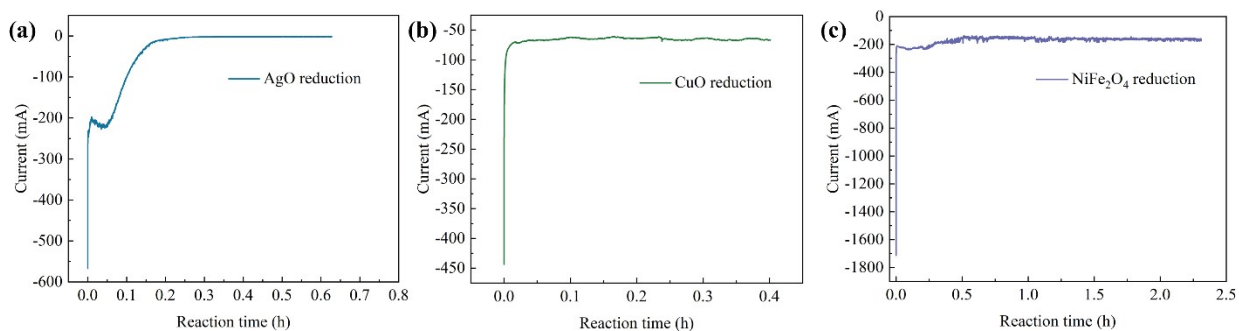
Fig. S10 Electrolysis current vs. reaction time plot of (a) AgO reduction, (b) CuO reduction, and (c) NiFe$_2$O$_4$ reduction.

Table S1 BET surface area of initial Fe_2O_3 and Fe_2O_3/C aggregates.

Sample	BET surface area (m^2/g)
Fe_2O_3	58.71
Fe_2O_3/C aggregates	149.13

Table S2 Comparison of iron production via electrolysis methods

Iron feedstock	Method	Conditions	Efficiency	References
Fe_2O_3	**Electronically-ionically conductive colloidal electrodes with Ni foam electrode**	**18 M NaOH, 100°C**	**>95%**	**This work**
Fe_2O_3	Pellet	NaCl-CaCl$_2$ molten salt, 800°C	~95.3%	[3]
Fe_2O_3	Pellet	Na$_2$CO$_3$–K$_2$CO$_3$ eutectic salt, 750°C	~93.6%	[4]
Fe_2O_3	Suspension with	18 M NaOH,	~95%	[5]

	carbon rotating disc electrode	114°C		
Iron ore	The pellet with metal wire	18 M NaOH, 100°C	~60%	[6]
Fe_2O_3	Pellet	Molten oxide electrolyte, 1550°C	~50%	[7]
Fe_2O_3	Pellet with Ni foil electrode	10 M NaOH, 90°C	~40%	[8]
Fe_2O_3	Suspension with graphite rod electrode	18 M NaOH, 110°C	~86%	[9]
Fe_3O_4	Pellet with Ni foil electrode	10 M NaOH, 90°C	~85%	[10]
Fe_2O_3	Suspension, graphite rotating disk	18 M NaOH, 110°C	~95%	[11]

Fe_2O_3	The pellet with copper rod electrode	Water mediator in molten LiCl, 660°C	~96%	[12]
Fe_2O_3	Pellet with Ni wire cathode	$CaCl_2$, 800°C	~80%	[13]
Fe_2O_3	Pellet with iron wire	Na_2CO_3–K_2CO_3 eutectic salt, 750°C	95%	[14]
Fe_2O_3	Table with Ni basket	Molten NaOH, 530°C	~90%	[15]
Fe_2O_3	Pellet	Molten NaOH, 500°C	~41.2%	[16]
Fe_2O_3	Powder	H_2 reduction, 850°C	35.8%	[17]
Fe_2O_3	Powder	CO reduction, 850°C	33.2%	[17]

| Fe$_2$O$_3$ | Powder | Carbon coal, N$_2$ gas, 1200°C | <30% | [18] |

Table S3 Mass of Fe produced and deposited Fe on Ni foam

Mass of slurry (g)	Mass of Fe2O3 in slurry (mg)	Mass of Fe produced theoretically (mg)	Mass of Ni foam before reaction (g)	Mass of Ni foam after reaction (g)	Mass of Fe on Ni foam (mg)	Mass of powder Fe/C produced (mg)	%Fe purity from powder	% Fe on Ni foam
1.21	163.35	122.38	0.5347	0.5704	35.4	40.7	95%	29%

According to the concern about Fe deposition on Ni foam, which could be problematic for production yield in large-scale production, we believe that effective approaches to prevent this deposition are supposed to be advanced. Currently, we are trying to solve this problem through some possible pathways. For example, a non-metallic/magnetic porous substrate such as porous C-based electrodes would help mitigate the electromagnetic interaction between Fe and Ni during electroreduction, which could help collect the Fe product more easily with less Fe deposition on C-based electrodes. Continuous flow electrolysis by flowing the Fe$_2$O$_3$ through the Ni foam substrate could possibly help reduce Fe deposition on Ni foam. By utilizing the flow system, the reduction of Fe$_2$O$_3$ to Fe is dynamical, as Fe$_2$O$_3$/C aggregates in the slurry need to move through the conductive Ni foam all the time, preventing sedimentation of Fe$_2$O$_3$/C on Ni foam surface. Hence, there might be less tendency for such a deposition compared to statically reducing Fe$_2$O$_3$ to Fe, as in the current static cell design. These solutions are worth further study to tackle the problem.

Regarding the yield of Fe in Table S3, the product that can be obtained from the small-scale reaction is around 40.7 mg of Fe/C. The Fe deposited on Ni accounts for 29%. However, we would like to note that it is challenging to accurately quantify the amount of recovered Fe mass. This is because there is unpredictable mass loss during the product collection, filtration, and separation processes. From our point of view, the product yield evaluation in the large-scale process with reliable separation equipment such as a centrifugal bowl and a magnetic separation machine, as we proposed in the flow process part, would be more accurate. In addition, the equipment used in the separation process in the flow process has more accurate efficiency (based on the specifications from the seller).

Table S4 ICP-OES results of electrolyzed Fe.

Sample	Calculated concentration of Fe (mg/L)	Tested concentration of Fe (mg/L)
Commercial Fe	285.714	292.688
Electrolyzed Fe	285.714	292.132

Note that the obtained numbers are within the 5% acceptable error range of ICP-OES. The concentration of electrolyzed Fe is insignificantly different from commercial Fe (Sigma Aldrich, 99.9%, metal basis) indicating high purity Fe produced by the LTE process.

Table S5 Base case scenario for the cost analysis used in this work.

	Base case condition
Fe_2O_3 content in source (wt%)	88.6
C black in the colloid (wt%)	10
Additives in the colloid (wt%)	0.1
Fe_2O_3 price ($/ton)	120

Electricity ($/kWh)	0.05
C black separation efficiency (%)	99
NaOH recycle efficiency (%)	99
Fe_2O_3 conversion efficiency (%)	95
Operating hour (h/year)	6240

Table S6 Analyzed annual cost breakdowns.

Fixed operating costs (FOC)	Annual cost ($/year)
Labor and overhead	2,403,753.22
Maintenance	961,156.95
Insurance	273,464.65
Total FOC	3,638,374.81
Variable operating costs (VOC)	**Annual cost ($/year)**
Fe_2O_3	12,000.000.00
C black powder	397,860.03
NaOH	976,240.74
Water	10,149.60
Electricity	7,646,956.00
Total VOC	21,225,842.28
Total product cost (TPC) = FOC + VOC	24,864,217.09

Note the total product cost (TPC) refers to the overall costs required for iron production at the set rate annually.

Table S7 CO_2 emissions from different electricity sources

Electricity sources	CO$_2$ emission (Kg/KWh)	References
Coal	1.04	[19]
Natural gas	0.44	[19]
Solar	0.05	[20]
Wind	0.011	[21]
Hydroelectric	0.0185	[22]
Biomass	0.23	[23]
Geothermal	0.038	[23]
Petroleum	1.08	[19]
Nuclear	0.012	[23]

Table S8 CO_2 emissions from material production

Electricity sources	CO$_2$ emission (Kg/Kg material produced)	References
Carbon black	2.38	[24]
NaOH	0.42	[24]
Na$_2$S	3.02	[25]

Notes and references

1. Q. Wang, B. Fu and Y. Wang, *Journal of The Electrochemical Society*, 2017, **164**, E428-E433.

2. Q. Wang and Y. Wang, *ACS Appl Mater Interfaces*, 2016, **8**, 10334-10342.

3. H. Li, L. Jia, J.-l. Liang, H.-y. Yan, Z.-y. Cai and R. G. Reddy, *International Journal of Electrochemical Science*, 2019, **14**, 11267-11278.

4. D. Tang, H. Yin, W. Xiao, H. Zhu, X. Mao and D. Wang, *Journal of Electroanalytical Chemistry*, 2013, **689**, 109-116.

5. B. Yuan and G. M. Haarberg, *ECS Transactions*, 2009, **16**, 31.

6. A. Allanore, H. Lavelaine, G. Valentin, J. Birat and F. Lapicque, *Journal of the Electrochemical Society*, 2008, **155**, E125.

7. J. Wiencke, H. Lavelaine, P.-J. Panteix, C. Petitjean and C. Rapin, *Journal of Applied Electrochemistry*, 2018, **48**, 115-126.

8. Y. A. Ivanova, J. Monteiro, L. Teixeira, N. Vitorino, A. Kovalevsky and J. Frade, *Materials & Design*, 2017, **122**, 307-314.

9. V. Feynerol, H. Lavelaine, P. Marlier, M.-N. Pons and F. Lapicque, *Journal of Applied Electrochemistry*, 2017, **47**, 1339-1350.

10. J. Monteiro, Y. A. Ivanova, A. Kovalevsky, D. Ivanou and J. Frade, *Electrochimica Acta*, 2016, **193**, 284-292.

11. M. Tokushige, O. E. Kongstein and G. M. Haarberg, *ECS Transactions*, 2013, **50**, 103.

12. K. Xie and A. R. Kamali, *Green Chemistry*, 2019, **21**, 198-204.

13. G. Li, D. Wang and Z. Chen, *Journal of Materials Sciences and Technology*, 2009, **25**, 767.

14.   H. Yin, D. Tang, H. Zhu, Y. Zhang and D. Wang, *Electrochemistry communications*, 2011, **13**, 1521-1524.

15.   A. Cox and D. J. Fray, *Journal of Applied Electrochemistry*, 2008, **38**, 1401-1407.

16.   D. Tian, H. Jiao, J. Xiao, M. Wang and S. Jiao, *Journal of Alloys and Compounds*, 2018, **769**, 977-982.

17.   G. Sun, B. Li, W. Yang, J. Guo and H. Guo, *Energies*, 2020, **13**, 1986.

18.   Z. Chen, C. Zeilstra, J. van der Stel, J. Sietsma and Y. Yang, *Ironmaking & Steelmaking*, 2020, **47**, 741-747.

19.   EIA, How much carbon dioxide is produced per kilowatthour of U.S. electricity generation?, https://www.eia.gov/tools/faqs/faq.php?id=74&t=11, (accessed 1/27, 2024).

20.   L. C. Stages, *J. Ind. Ecol*, 2012, 56.

21.   M. Ozoemena, W. M. Cheung and R. Hasan, *Clean Technologies and Environmental Policy*, 2018, **20**, 173-190.

22.   M. Pang, L. Zhang, C. Wang and G. Liu, *The International Journal of Life Cycle Assessment*, 2015, **20**, 796-806.

23.   LowCarbonPower, Where do our emissions numbers come from?, https://lowcarbonpower.org/blog/emissions?fbclid=IwAR2jnNOgDaFuqqM0Z-fDhNoS46TheU-nq-f7LYhr-9FvVlADe7EJxFpbK8Q, (accessed 1/27, 2024).

24.   Veolia, *WSTP south end plant process selection report - Appendix H CO2 emission factors database.*, 2011.

25.   K. E. Tomberlin, R. Venditti and Y. Yao, *BioResources*, 2020, **15**, 3899-3914.